Applications and Applied Mathematics: An International Journal (AAM)

Volume 19 | Issue 1 Article 6

12-2023

(R2055) Magnetic Effects on Unsteady Non-Newtonian Blood Flow through a Tapered and Overlapping Stenotic Artery

Abiodun J. Babatunde
The University of Ilorin

Moses S. Dada
The University of Ilorin

Available at
http://pvamu.edu/aam
Appl. Appl. Math.
ISSN: 1932-9466

Applications and Applied Mathematics:
An International Journal
(AAM)

Vol. 19, Issue 1 (June 2024), Article 6, 19 pages

Magnetic Effects on Unsteady Non-Newtonian Blood Flow through a Tapered and Overlapping Stenotic Artery

[1*]Abiodun J. Babatunde and [2]Moses S. Dada

Department of Mathematics
Faculty of Physical Science
University of Ilorin
Ilorin, Nigeria
[1]babatundeabiodunjoseph@gmail.com and [2]dadamsa@gmail.com

*Corresponding Author: babatundeabiodunjoseph@gmail.com

Received: December 26, 2022; Accepted: January 23, 2024

Abstract

This study aims to investigating the effect of magnetic field and porosity on non-Newtonian flow of blood through a tapered, and overlapping stenosed artery. The Casson fluid model represents the rheological character of blood. A tapered and overlapping stenosed artery influences the hemodynamic behavior of the blood flow. The problem is solved by using analytical techniques with the help of boundary conditions, and results are displayed graphically for different flow characteristics like pressure drop, shear stress, velocity profile and stream function. It is realized that rises in Darcy number and Womersley number accelerates the velocity profile and reduces the radial direction, but increases in magnetic field reduces the velocity profile. The pressure drop is increasing with an increase in magnetic field and Womersley number but drops with an increase in the value of Darcy number. The wall shear stress is increasing with an increase in the value of magnetic field, at a stenosis region but converse at a non-stenosis region, it drops by ascending in the value of Darcy number, and increases as Womersley number rising, and the wall shear stress decelerate as tapered angle rises. The interesting outcomes collected in this literature review and survey conducted can aid the medical practitioners to predict blood movement in an atherosclerotic arteries. More so, from this study we discovered that magnetic field parameter possesses the ability to reduce viscosity of the blood, a leading cause of heart attack, strokes, anaemia and many other cardiovascular diseases

Keywords: Non-Newtonian flow; Casson fluid; Wall shear stress; Stream function; Pressure drop; Blood flow; Overlapping stenosis artery

MSC 2010 No.: 76Z05, 74L15

1. Introduction

The process of progressive thickening and hardening of the walls of medium-sized and large arteries due to cholesterol on their inner lining is called atherosclerotic. The stenosis of an artery could be caused by high cholesterol when it grows on the artery's inner wall. This buildup, referred to as atherosclerosis, can accumulate within the artery to an extent where it reduces blood flow to organs of the body. When blood flow is reduced, oxygen and nutrients cannot travel to the tissues that need it, which can lead to many coronary artery diseases such as heart attack, strokes, and peripheral vascular diseases, which has been the significant causes of death in the world. The importance of the hemodynamic factors played a significant role at the beginning and the propagation of atherosclerosis which took the attention of Mann et al. (1938). Stenosis growth problems under various fluid flow situations have been addressed by many researchers such as Keane et al. (2003), said stenosis could be regarded generally as an abnormal narrowing of a body passage (Kuzma et al. (2018)). The restriction in blood supply to tissues, causing a shortage of oxygen needed (by the brain) for cellular metabolism, is called ischemia. It can be because of stenosis (obstruction) in the blood vessel, supplying the blood in that part. Sherwood (2016), observed that stenosis is a significant cause of serious circulatory disorders, affecting many hydrodynamic factors like resistance to flow, wall shear stress, and apparent viscosity. Aortic stenosis, Hypertrophic subaortic stenosis, Mitral stenosis, Pulmonary stenosis, Renal artery stenosis, Spinal stenosis, Subaortic stenosis, Tracheal stenosis, Tricuspid stenosis are common types of stenosis.

Newtonian and non-Newtonian fluids are ubiquitous in industries and medicine processes. The blood exhibits as a non-Newtonian fluid when it flows through vessels with a smaller radius at a low shear rate, whereas it behaves as a Newtonian fluid while flowing through vessels with a larger radius at a high shear rate (Eldesoky (2012); Jain et al. (2011)). Taylor (1959) observed that at low shear (lower than 100s−1) rate, blood behaves as a non-Newtonian fluid flow and at a high shear rate (1000s−1), blood exhibits Newtonian fluid flow property in large arteries like the aorta. A low shear rate is noticed in the stenotic region, and blood flow through the stenosed artery behave like non-Newtonian characteristics. Moreno and Bhanagar (2013) modelled realistic physiological flow conditions calculating for the unsteady flow conditions (systole/diastole) also with the movement from laminar to a turbulent state. Their analyzes clearly stated that, at the same level of stenosis, (i) the presence of turbulence, (ii) location of movement to turbulence, (iii) turbulence intensity, and (iv) region of turbulence are type-dependent. Prakash et al. (2015) studied the effects of stenosis on non-Newtonian flow of blood in blood vessels. The effect of stenotic geometry and non-Newtonian property of blood flow through arterial stenosis was examined by Somchai Sriyab (2020).

Many researchers think that the hydrodynamic factors can help in the fundamental understanding, diagnosis and treatment of these disorders. Verma et al. (2004) observed the shape of stenosis to blood flow through an artery with mild stenosis and concluded that for a constant flow rate, the wall shear stress rises as the stenosis increases in size. Misra and Shit (2006) studied the blood flow through the arterial segment, taking blood flow as Hershal-Bulkley fluid. They discovered that the skin friction, and the resistance to flow are maximum at the throat of the stenosis and minimum at the end. Ali et al. (2009) studied the effect of an axially symmetric time-dependent growth into the lumen of a tube for constant cross-section through which a Newtonian fluid is

steadily flowing. They observed the structure of flow through an arterial model with single or double sinusoidal stenosis, assuming that the arterial blood flow is quasi-steady. Shah and Siddiqui (2011) analyzed the influence of peripheral layer viscosity on physiological characteristics of blood flow through a stenosed artery using the Power-law fluid model. They found that the resistance to flow rises as stenosis size, and peripheral layer viscosity increases, and the peripheral layer viscosity of blood in diabetic patients is higher than in non-diabetic patients, resulting in higher resistance to blood flow. Thus, diabetic patients with higher peripheral layer viscosity are more prone to high blood pressure. Therefore, the resistance to blood flow in the case of diabetic patients may be reduced by reducing the viscosity of the plasma. They also, investigated that the wall shear stress decreases as the stenosis shape parameter increases, but in the case of increasing stenosis size, stenosis length, and peripheral layer viscosity, wall shear stress is increases. Mathematical modelling of Non-Newtonian blood flow through an artery in the Presence of Stenosis was analyzed by Pankaj and Surekha (2013). Argyropoulos and Markatos (2015) reviewed the recent advances and success of turbulent computing flows. Their review was primarily concerned with the most recent methods for computer predictions such as Direct Numerical Simulation (DNS) and Large Eddy Simulation (LES) to flow in pipes and free-surface flows. They noticed that the LES was the most accurate among the methods available for practical computations. In favor of the above work, Hye and Paul (2015) proposed that the spiral effect should be incorporated to get a better insight into the transition-to-turbulence flow of blood through arterial stenosis. Their results showed that the spiral flow affected the turbulence kinetic energy in the post stenosis region, and the wall pressure and shear stress remained almost unchanged by the spiral velocity. Mahalingam et al. (2016) studied the nature of blood flow through stenosed coronary arteries by numerical analysis of the effect of turbulence transition on the hemodynamics parameters. They found that the primary biological effect of blood turbulence is the change in wall shear stress on the endothelial cell membrane, while the local oscillatory nature of the blood flow influences some physiological changes in the coronary artery. Thakur et al. (2018) used a fluid hydrodynamic model in the magnetized plasma sheath in a cylindrical coordinate system. Puskar et al. (2020) examined the analysis of blood flow through the artery with mild stenosis. Aniruddha et al. (2022) explored mathematical modelling of pulsatile blood in straight rigid artery system.

Magnetohydrodynamics (MHD) is to study of the magnetic properties and behavior of electrically conducting fluids. The magnetic field with Newtonian fluid and non-Newtonian fluids has broad applications in bio-fluid mechanics, chemical engineering and various industries. If a magnetic field is applied to an electrically conducting liquid in motion, it induces electric and magnetic fields. Radiative heat transfer to blood flow through a stenotic artery in the presence of erythrocytes and magnetic field was investigated by Prakash and Makinde (2011). Chinyoka and Makinde (2014) examined the computational dynamic of arterial blood flow in the presence of magnetic field and thermal radiation therapy. Dada and Alamu (2020) studied heat and mass transfer in blood flow through a tapered artery with mild stenosis. They discovered that the temperature blood rises as micropolar spin parameter increases and its concentration is drop with an increase in the micropolar parameter or coupling number. Das et al. (2021) looked at Hall and ion slip currents impact on electromagnetic blood flow conveying hybrid nanoparticles through an endoscope with peristaltic waves. Hemodynamical analysis of MHD two phase blood flow through a curved permeable artery having variable viscosity with heat and mass transfer was studied by Sharma et al. (2022).

In a case of overlapping, there is a suturing of a layer of tissue above or under another in order to gain strength. Mathematical modelling of blood flow through overlapping arterial stenosis was examined by Chakravarty and Mandal (1994), who observed that the severity of the overlapping stenosis affects the resistance to flow greatly. The flux is inversely proportional to the resistive impedance arising out of the stenotic flow in vivo, and that the wall shear stress is inversely proportional to the amplitude of the pressure gradient. Srivastava et al. (2010) analyzed the increased impedance and other flow characteristics during artery catheterization with composite stenosis, assuming that the flowing blood behaves like a Newtonian fluid. Mathematical modelling of blood flow through three-layered stenosed artery analyzed by Sapna et al. (2017). Babatunde and Dada (2021) studied the effects of hematocrit level on blood flow through an overlapping stenosed artery with porosity. Afiqah and Sankar (2023) did a review on non-Newtonian fluid models for multilayered blood rheology in constricted arteries.

In the present work, the blood flow through an artery was described by Navier-Stokes equations which were presented along with the continuity equation in cylindrical form as the model employed, and Casson fluid model is used to simulate the rheological characteristics of blood flow.

The new research work has combined the effects of magnetic field, porosity and non-Newtonian flow through a tapered, and overlapping stenosed artery has not been considered to the best knowledge of the authors.

2. Formulation of the Problem

The blood flow is modelled in arteries by Navier-Stokes equations for fluid flow through a cylinder (Young (1968) and Kapur (1985)). Let the three components of velocities along the radius vector, perpendicular to the radius vector, and parallel to the axis of z, be w^r, w^θ, and w^z , respectively,

$$\frac{1}{r}\frac{\partial}{\partial r}(rw^r) = -\frac{\partial}{\partial z}(rw^z), \tag{1}$$

$$\frac{\partial p}{\partial r} + \rho\left(\frac{\partial w^r}{\partial t} + w^r\frac{\partial w^r}{\partial z} + w^z\frac{\partial w^r}{\partial z}\right) = \mu\left(\frac{\partial^2 w^r}{\partial r^2} + \frac{\partial^2 w^r}{\partial z^2} + \frac{1}{r}\frac{\partial w^r}{\partial r} - \frac{w^r}{r^2}\right) \tag{2}$$

$$\frac{\partial p}{\partial z} + \rho\left(\frac{\partial w^z}{\partial t} + w^r\frac{\partial w^z}{\partial r} + w^z\frac{\partial w^z}{\partial z}\right) = \mu\left(\frac{\partial^2 w^z}{\partial r^2} + \frac{\partial^2 w^z}{\partial z^2} + \frac{1}{r}\frac{\partial w^z}{\partial r}\right) - \mu\left(\frac{1}{k'} + {\beta_0}^2\sigma\right)w^z, \tag{3}$$

where r, μ, ρ, p, k', β_0, and σ are the radius of the artery (m), dynamic viscosity of the blood (pa.s), density of the blood sample (kg/m^3), pressure (pam^{-1}), permeability of Porous medium, intensity of magnetization, and electric conductivity of the blood, respectively.

2.1 The constitutive relations

The Casson fluid model was implemented to capture the rheological effects of the blood (Kim et al. (2009)). The constitutive relations between an initial yield stress and Casson fluid model term becomes:

$$\sqrt{\tau} = \sqrt{k} \times \sqrt{\dot{\gamma}} + \sqrt{\tau_y} \quad \text{when} \quad \tau \geq \tau_y, \tag{4}$$

and

$$\dot{\gamma} = 0 \quad \text{when} \quad \tau \geq \tau_y, \tag{5}$$

τ_y is the yield stress (N.m^{-2}), $\dot{\gamma}$ is shear rate (s^{-1}), k is Casson model constant (Pa.s), respectively.

The mathematical expression for the geometry (Figure 1) of the present problem is given as Mekheimer and El Kot (2012),

$$\frac{R(z,t)}{R_0} = \begin{cases} \left(\frac{\zeta z}{R_0} + 1\right) - \frac{\delta cos\emptyset}{R_0 L_0}(z-d)\left\{11 - \frac{94}{3L_0}(z-d) + \frac{32}{L_0^2}(z-d)^2 \right. \\ \left(\frac{\zeta z}{R_0} + 1\right)\Omega(\mathrm{t}), \end{cases} \quad \begin{matrix} \\ otherwise, \end{matrix} \tag{6}$$

$$\left. - \frac{32}{3L_0^3}(z-d)^3\right\}\Omega(\mathrm{t}), d \leq z \leq d + \frac{3L_0}{2},$$

the time dependent parameter $\Omega(\mathrm{t})$ is given by

$$\Omega(\mathrm{t}) = 1 - \mathrm{a}(\cos\omega\mathrm{t} - 1)\mathrm{e}^{[-\mathrm{a}\omega\mathrm{t}]}, \tag{7}$$

where R(z, t) represents the radius of the tapered arterial segment in the constricted region, R_0 represents the constant radius of the normal artery in the absence of stenosis, φ is the tapered angle, $\frac{3L_0}{2}$ is the length of overlapping stenosis, d is the location of the stenosis, δcosφ is taken to be the critical height of the overlapping stenosis, and $\zeta = (\tan\varphi)$ represents the slope of the tapered vessel. Categorizing φ<0 as converging tapering, φ=0 as non-tapered artery and φ>0 as the diverging tapering in order to explore the possibility of the different shapes of the artery.

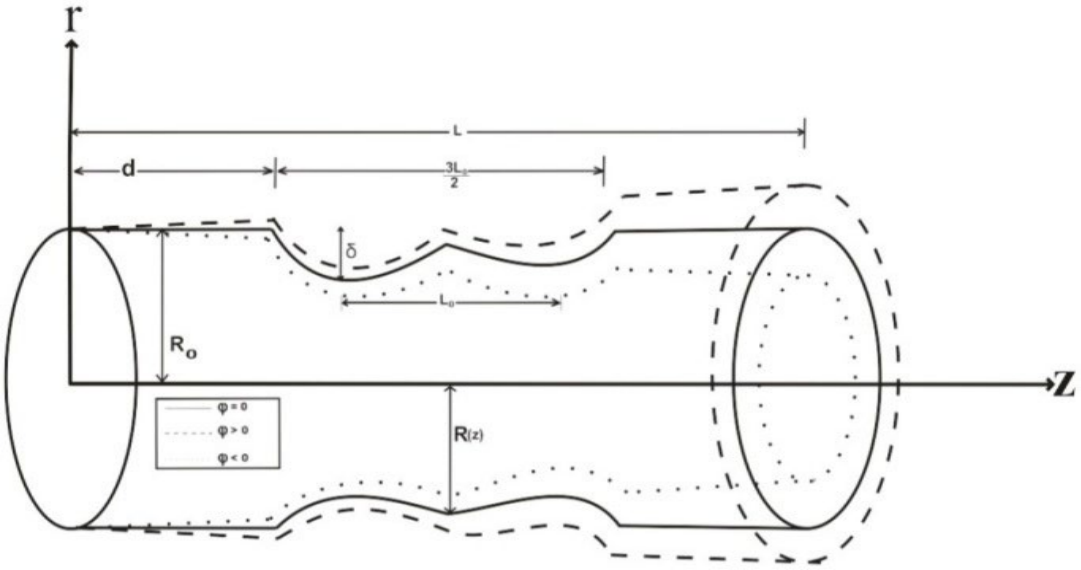

Figure 1. Geometry of the problem

Consider an axisymmetric, unsteady and fully developed flow of blood through a circular cylindrical tube, i.e., $w^{\theta} = 0, \frac{\partial w^{z}}{\partial z} = 0$, and $w^{r} = w_0$. Take the blood flow as non-Newtonian fluid for small vessel system. The vessel with radius less than 0.05 mm can be treated as small vessel and dynamic viscosity (μ) in Equation (2) and can be modified in terms of effective viscosity (μ_{eff}) and can be evaluated in terms of initial yield stress applying Casson fluid model.

Equations (1) to (3) become

$$\rho \frac{dw_0}{dt} = -\frac{\partial p}{\partial z} + \mu_{eff}\left(\frac{\partial^2 w_0}{\partial r^2} + \frac{1}{r}\frac{\partial w_0}{\partial r}\right) - \mu_{eff}\left(\frac{1}{k\prime} + \beta^2 \sigma a^2\right) w_0, \tag{8}$$

where w_0 is the velocity of the blood flow, and μ_{eff} is the effective viscosity.

The following non-dimensional variables are introduced to simplify the governing model equations are:

$$\bar{z} = \frac{z}{R_0}; \bar{r} = \frac{r}{R_0}; \ \bar{w} = \frac{w_0}{W_\infty}; Da = \frac{k\prime}{R_0^2}; \ M = \beta_0 R_0 \sqrt{\sigma}; \bar{t} = t \times \omega; \ \bar{p} = \frac{p}{\rho W_\infty^2}, \tag{9}$$

where z is the dimensional axial position (mm), R_0 is the constant radius of the normal artery in the absence of stenosis (mm), r is the dimensional radial position (mm), w is the velocity (m/s), W_∞ is the average velocity (m/s), t is the time, ω is the oscillating frequency (rad/s). The Non-dimensional variables are represented with bar.

Substituting Equation (9) into Equation (8) resulted to the non-dimensional form as:

$$\rho W_\infty \omega \left(\frac{d\bar{w}}{d\bar{t}}\right) = -\frac{\rho W_\infty^2}{R_0}\frac{\partial \bar{p}}{\partial \bar{z}} + \mu_{eff}\frac{W_\infty}{R_0^2}\left(\frac{\partial^2 \bar{w}}{\partial \bar{r}^2} + \frac{1}{\bar{r}}\frac{\partial \bar{w}}{\partial \bar{r}}\right) - \mu_{eff}\frac{W_\infty}{R_0^2}\left(\frac{1}{Da} + M^2\right)\bar{w}, \quad (10)$$

with the boundary conditions

$$\bar{w} = 0 \text{ at } \bar{r} = \frac{R(z,t)}{R_0}, \text{ (no-slip condition)} \quad (11)$$

$$\bar{w} = 0 \text{ at } \bar{r} = 0, t \geq 0. \quad (12)$$

Dividing through by $\mu_{eff}\frac{W_\infty}{a^2}$ resulted to:

$$\alpha^2\left(\frac{d\bar{w}}{d\bar{t}}\right) = -Re\frac{\partial \bar{p}}{\partial \bar{z}} + \left(\frac{\partial^2 \bar{w}}{\partial \bar{r}^2} + \frac{1}{\bar{r}}\frac{\partial \bar{w}}{\partial \bar{r}}\right) - \left(\frac{1}{Da} + M^2\right)\bar{w}, \quad (13)$$

where $\alpha = R_0\left({}^{\omega\rho}/_{\mu_{eff}}\right)^{\frac{1}{2}}$ and $Re = {}^{W_\infty \rho R_0}/_{\mu_{eff}}$,
α is the Womersley number and Re is the Reynolds number

3. Analysis

Pulsatile pressure gradient may be expressed in terms of frequency and time limit for an unsteady state,

$$\frac{\partial \bar{p}}{\partial \bar{z}} = -P_0 e^{-i\omega t}, \quad (14)$$

the pumping action of the heart gives rise to oscillatory flow of the blood. We assume

$$\bar{w}(r,t) = \bar{w}(r)_0 e^{-i\omega t} \ . \quad (15)$$

The corresponding boundary conditions:

$$\bar{w}_0 = 0 \quad \text{at } \bar{r} = R(z,t), \text{ (no-slip condition)} \quad (16)$$

$$\bar{w}_0 = 0 \quad \text{at} \quad \bar{r} = 0, t \geq 0, \quad (17)$$

where $\gamma^2 = \alpha^2\left(\frac{1}{Da} + M^2 + i\omega\right)$.

Applying the transformation $h = \frac{\bar{r}}{R(z,t)}$ in the Equations (13), (16), and (17) we have:

$$\left(h^2\frac{\partial^2 \bar{w}_0}{\partial h^2} + h\frac{\partial \bar{w}_0}{\partial h}\right) - \gamma^2 h^2 \bar{w}_0 = R(z,t)^2 ReP_0, \quad (18)$$

$$\bar{w}_0 = 0 \quad \text{at } h = 1, \quad (19)$$

$$\bar{w}_0 = 0 \text{ at } h = 0, t \geq 0. \quad (20)$$

Now, the homogeneous solution of Equation (18) is:

$$\left(h^2\frac{\partial^2 \bar{w}_0}{\partial h^2} + h\frac{\partial \bar{w}_0}{\partial h}\right) - \gamma^2 h^2 \bar{w}_0 = 0. \quad (21)$$

The above Equation (21) is a modified Bessel differential equation; therefore, its solution can be given as:

$$\bar{w}_0(h) = C_1 I_0(\gamma h) + C_2 K_0(\gamma h)\ , \quad (22)$$

$C_2 = 0$, as the solution is bounded at $h = 0$. Hence, Equation (22) is modified as:

$$\bar{w}_0(h) = C_1 I_0(\gamma h) \, . \tag{23}$$

The particular solution of Equation (18) in terms of velocity, which gives:

$$\bar{w}_{0p}(h) = \frac{R(z,t)^2 ReP_0}{\gamma^2} \, . \tag{24}$$

The general solution is obtained by adding Equations (24) and (23) together:

$$\bar{w}_{0g} = C_1 I_0(\gamma h) + \frac{R(z,t)^2 ReP_0}{\gamma^2} \, . \tag{23}$$

In order to solve arbitrary coefficient C_1 in Equation (21), the boundary condition based on Equation (20) can be modified as:

$$C_1 = -\frac{R(z,t)^2 ReP_0}{\gamma^2} \, . \tag{24}$$

The complete solution of Equation (18) in terms of non-dimensional pulsating velocity profile as a function of non-dimensional radial position can be obtained as:

$$\bar{w} = \left[\frac{R(z,t)^2 ReP_0}{\gamma^2}\left(2 - I_0(\gamma h)\right)\right] e^{-i\omega t} \, . \tag{25}$$

The volumetric flow rate, Q, is defined as

$$Q = \int_0^{R(z,t)} 2\pi \bar{r} \bar{w} d\bar{r} \ \ . \tag{26}$$

After substituting Equation (25) into Equation (26), and integrating, we have

$$Q = \ 2\pi \frac{R(z,t)^2 ReP_0}{\gamma^2} e^{-i\omega t} \int_0^{R(z,t)} \bar{r} \left[\left(2 - I_0(\gamma h)\right)\right] d\bar{r} \, . \tag{27}$$

After simplification, we have:

$$Q = 2\pi e^{-i\omega t} \frac{R(z,t)^2 ReP_0}{\gamma^2} \left[R(z,t)^2 - R(z,t) I_1(\gamma h)\right] . \tag{28}$$

Then, the pressure gradient can be written as:

$$\frac{\partial p}{\partial z} = \frac{Q\gamma^2}{2\pi R(z,t)^2 Re[R(z,t)^2 - R(z,t) I_1(\gamma h)]} \, . \tag{29}$$

Integrating Equation (29) along the length of the artery and using the condition that $P = P_0$ at $z = 0$ and $P = P_1$ at $P = L$, we obtain:

$$P_1 - P_0 = \frac{Q\gamma^2}{2\pi Re} \int_0^L (R(z,t))^{-1} [R(z,t) - I_1(\gamma h)]^{-1} dz \, , \tag{30}$$

where $\frac{R(z,t)}{R_0}$ is given by Equation (6).

The pressure drop along the length of the stenotic region is

$$\Delta P = \frac{Q\gamma^2}{2\pi Re}\int_d^{d+\frac{3}{2}L_0}(R(z,t))^{-1}[R(z,t)-I_1(\gamma h)]^{-1}dz\,. \tag{31}$$

If there is no stenosis, hence $\delta = 0$, from Equation (6) $\left(R(z,t) = (\zeta z + R_0)\Omega(\mathrm{t})\right)$,

$$(\Delta P)_N = \frac{Q\gamma^2}{2\pi Re}\int_0^L\left((\zeta z + R_0)\Omega(\mathrm{t})\right)^{-1}[(\zeta z + R_0)\Omega(\mathrm{t}) - I_1(\gamma h)]^{-1}dz. \tag{32}$$

The pressure drop in non-dimensional form is given by

$$\bar{P} = \frac{\Delta P}{(\Delta P)_N} = \frac{\int_d^{d+\frac{3}{2}L_0}(R(z,t))^{-1}[R(z,t)-I_1(\gamma h)]^{-1}dz}{\int_0^L\left((\zeta z+R_0)\Omega(\mathrm{t})\right)^{-1}[(\zeta z+R_0)\Omega(\mathrm{t})-I_1(\gamma h)]^{-1}dz}\,. \tag{33}$$

The wall shear stress is denoted by τ and given by Puskar et al. (2020) and Babatunde and Dada (2021) as:

$$\tau_R = -\frac{R}{2}\frac{\partial p}{\partial z} = -\frac{Q\gamma^2}{4\pi R_0^2\left(\frac{R(z,t)}{R_0}\right)^2 Re\left[R_0\left(\frac{R(z,t)}{R_0}\right)-I_1(\gamma h)\right]}\,. \tag{34}$$

Also, in the absence of stenosis in the artery $\frac{R(z)}{R_0} = \left(\frac{\zeta z}{R_0}+1\right)\Omega(\mathrm{t})$, then, skin-friction of normal artery can be expressed as:

$$\tau_N = -\frac{Q\gamma^2}{4\pi R_0^2\left(\left(\frac{\zeta z}{R_0}+1\right)\Omega(\mathrm{t})\right)^2 Re\left[R_0\left(\left(\frac{\zeta z}{R_0}+1\right)\Omega(\mathrm{t})\right)-I_1(\gamma h)\right]}\,. \tag{35}$$

In dimensionless form, the skin-friction can be expressed as:

$$\bar{\tau} = \frac{\tau_R}{\tau_N} = \frac{\left(\left(\frac{\zeta z}{R_0}+1\right)\Omega(\mathrm{t})\right)^2\left[R_0\left(\left(\frac{\zeta z}{R_0}+1\right)\Omega(\mathrm{t})\right)-I_1(\gamma h)\right]}{\left(\frac{R(z,t)}{R_0}\right)^2\left[R_0\left(\frac{R(z,t)}{R_0}\right)-I_1(\gamma h)\right]}\,. \tag{36}$$

The streamline flow in fluid dynamic can be defined as the flow in which the fluids flow is in separate layers without disruption or coarse of the layers and at a given point, the velocity of each fluid particle moving by remains constant with time. The movement of particles of the fluid follows a certain order with respect to the particles moving in a straight line parallel to the pipe wall in a way that the adjacent layers slide past each other like playing cards. The stream function (ψ) of the blood flow can be obtain mathematically as integral of $w = \frac{1}{r}\frac{\partial\psi}{\partial r}$ with $\psi = 0$ at $r = R(z,t)$, then the stream function is given by:

$$\psi = \int_0^{R(z,t)} rwdr = e^{-i\omega t}\frac{R(z,t)^2 ReP_0}{\gamma^2}\left[R(z,t)^2 - R(z,t)I_1(\gamma h)\right]\,. \tag{37}$$

4. Results and discussions

In this section, stimulation of the effects of blood flow parameters have been shown. From Das et al. (2021) and Babatunde and Dada (2021) and others, the values for the parameters are taken. The values of the parameters are considered with its range as Re = 0.2, Q = 0.1, L = 3, Da=0.2-0.4, M=1-3, z = 1.5, t = 0.2-0.5, $R_0 = 0.5$, P_0= 0.3, $\omega = 0.1$, $\delta = 0.02 - 0.3$ and $\theta = 0$. Womersley number (α) in cardiovascular system for a canine of the heart rate 2Hz are ascending aorta is 13.2, descending aorta is 11.5, abdominal aorta is 8, femoral artery is 3.5, carotid artery is 4.4, arterioles is 0.04. The viscosity of blood for normal adult is 0.3 millipoise.

The results obtained in this work comprises the expression for velocity profile in Equation (25), the expression for pressure drop in Equation (33), expression for wall shear stress in Equation (36), and the stream function of the blood in Equation (37), and the graphs were shown. Figure 2 displays the variation of velocity profile against *r* for different values of Darcy number, Da. It is observed that increases in Darcy number enhances the velocity profile and decreases the radial direction, *r*. Figure 3 displays the variation of velocity profile against *r* for different values of Magnetic field, (M). It is observed that increases in magnetic field reduces the velocity profile. It happens because magnetic field on blood flow increases the internal viscosity of the blood flow which causes rise in the Lorentz force. Figure 4 displays the variation of velocity profile against *r* for different values of Womersley number. It can be seen that velocity reduces as the value of Womersley number increases. Figure 5 depicts the variation of velocity profile against *r* for different values of Reynold number. A rise in Reynold number increases the velocity profile. Figure 6 shows velocity against *r* for different values of time. An increment in time taken, t reduces the velocity profile. Figure 7 is the velocity against r for different values of tapered angle(φ). It depicts that velocity enhances by increases the values of tapered angle (φ). However, diverging tapering produces upper bound velocity and converging tapering results in lower bound velocity.

Figures 8, 9 and 10 depict the variation of pressure drop against stenosis height for different values of magnetic, M, Darcy number, Da, and Womersley number, α, respectively. They showed that the pressure drop is increasing with an increase in magnetic field, pressure drop reduces with an increase in the value of Darcy number, it also hake as the value of Womersley number, α rises. Figures 11, 12, 13, 14, and 15 depict the variation of wall shear stress against z for different values of magnetic, M, Darcy number, Da, Womersley number, α Tapered angle, φ and stenosis height, $\frac{\delta}{R_0}$, respectively. Figure 11 represents the variation of shear stress against z for different values of magnetic field, M. The wall shear stress is increasing with an increase in the value of magnetic field, at a stenosis region but converse is the case at non-stenosis region, it drops by ascending in the value of Darcy number, and increases as Womersley number rising, and the wall shear stress decelerate as tapered angle rises but accelerates as stenosis height moves up. Figures 16 and 17 display the streamline flows of the blood.

5. Conclusions

The effect of magnetic field on non-Newtonian porous blood flows through a tapered and overlapping stenotic artery was determined in this present study by considering blood flow through

the artery as Casson fluid flow. The resulting equations were solved analytically and are shown as follow:

i. It is found that a rise in the value of Darcy number enhances the velocity profile and decreases the radial direction. It happens because Darcy number on blood flow reduces the internal viscosity of the blood flow which causes decrease in the Lorentz force.
ii. It can be seen that increases in magnetic field and time reduces the velocity profile. However, blood flow in an applied magnetic field causes increase to induced voltages in the aorta and other major arteries of the central circulatory system that can be observed as superimposed electrical signals in the electrocardiogram.
iii. We observed velocity reduces as the value of Womersley number rises.
iv. It is observed that the rise in Reynold number increases the velocity profile. Moreover, low Reynolds number indicates the significant dominance of viscous forces over inertial forces, which keeps the flow in the laminar path.
v. It is found that the wall shear stress is increasing with an increase in the value of magnetic field and Womersley number but decrease in the value of tapered angle.
vi. It is also observed that wall shear stress drops by increment in the value of Darcy number.

This paper is capable of investigating under the purview of a single study the results for many models, such as the dilatant Casson fluid model, and the non-Newtonian viscous model. Moreso, this paper is very important for the purpose of simulation and validation of different fluid models in several cases of atherosclerosis.

REFERENCES

Afiqah, S. W. and Sankar, D. S. (2023). A review on non-Newtonian fluid models for multilayered blood rheology in constricted arteries, Arch Appl Mech., Vol. 93, No. 5, pp. 1771-1796.

Ali, R., Kaur, R., Katiyar, V. K. and Singh, M. P. (2009). *Mathematical Modeling of Blood Flow through Vertebral Artery with Stenoses,* Indian Society of Biomechanics, Special Issue NCBM, 0974-0783.

Aniruddha, B.P., Abbas, S. and Joydeb, M. (2022). Mathematical modelling of pulsatile blood in straight rigid artery system, Indian National Academy of Engineering, Vol. 9, No. 9, pp. 1-16.

Argyropoulos, C. D. and Markatos, N. C. (2015). Recent advances on the numerical modeling of turbulent flows, Applied Mathematical Modeling, Vol. 2, No. 39, pp. 693-732.

Babatunde, A. J. and Dada, M. S. (2021). Effects of hematocrit level on blood flow through a tapered and overlapping stenosed artery with porosity, Journal of Heat and Mass Transfer Research, Vol. 8, pp. 39-47.

Chakravarty, S. and Mandal, P. K. (1994). The Mathematical modelling of blood flow through an overlapping arterial stenosis, Mathematical and Computer Modelling, Vol. 19, No. 1, pp. 59-70.

Chinyoka, T. and Makinde, O.D. (2014). Computational dynamics of arterial blood flow in the presence of magnetic field and thermal radiation therapy, Advances in Mathematical Physics, Vol. 2014, Article ID 915640, 9 pages.

Dada, M. S. and Alamu-Awonira, F. (2020). Heat and mass transfer in micropolar model for blood flow through a stenotic tapered artery, Application and Applied Mathematics, Vol. 15, No. 2, pp. 1114-1134.

Das, S., Barman, B., Jana, R.N. and Makinde, O.D. (2021). Hall and ion slip currents impact on electromagnetic blood flow conveying hybrid nanoparticles through an endoscope with peristaltic waves, Bionano Science, Vol. 11, pp. 770-792.

Eldesoky, I. M. (2012). Slip effects on the unsteady MHD pulsatile blood flow through porous medium in an artery under the effect of body acceleration, International Journal of Mathematics and Mathematical Sciences, Vol. 8, No. 2, ID 860239, 26 pages.

Hye, Md. A., and Paul, M. C. (2015). A computational study on spiral blood flow in stenosed arteries with and without an upstream curved section, Applied Mathematical Modelling, Vol. 3, No. 9, pp. 4746-4766.

Jain, M., Sharma, G. C. and Singh R. (2010). Mathematical modeling of blood flow in a stenosed artery under the MHD effect through porous medium, International Journal of Engineering, Transactions B, Vol. 23, No. 3-4, pp. 243-251.

Kapur, J. N. (1985). *Mathematical Models in Biology and Medicine*, Affiliated East-West Press Pvt. Ltd., India, pp. 520.

Keane, M. and O'Toole, M. (2003). *Miller-Keane Encyclopedia and Dictionary of Medicine* (7^{th} Edition), Nursing & Allied Health, Elsevier.

Kim, S., Namgung, B., and Ong, P.K. (2009). Determination of rheological properties of whole blood with a scanning capillary-tube rheometer using constitutive models, J Mech Sci Technol., Vol. 23, pp. 17-18.

Kuzma, E., Lourida, I., Moore, S.F.D. (2018). Stroke and dementia risk: A systematic review meta-analysis, Alzheimer's & Dementia, Vol. 11, pp. 1416-1426.

Mahalingam, A., Gawandalkar, U. U., Kini, G., Buradi, A., Araki, T., Ikeda, N., Nicolaides, A., Laird, J.R., Saba, L. and Suri, J.S. (2016). Numerical analysis of the effect of turbulence transition on the hemodynamic parameters in human coronary arteries, Cardiovascular Diagnosis and Therapy, Vol. 6, No. 1, pp. 208-220.

Mann, F. C., Herrick, J. F., Essex, H. E. and Blades, E. J. (1938). Effects on blood flow of decreasing the lumen of blood vessels, Surgery, Vol. 4, pp. 249–252.

Mekheimer, Kh.S. and El Kot, M. A. (2012). Mathematical modelling of unsteady flow of a Sisko fluid through an anisotropically tapered elastic arteries with time-variant overlapping stenosis, Applied Mathematical Modelling, Vol. 36, pp. 5393-5407.

Misra, J.C. and Shit, G.C. (2006). Blood flow through arteries in a pathological state: A theoretical study, International Journal of Engineering Science, Vol. 44, pp. 662-671.

Moreno, C. and Baghanagar, K. (2013). Modeling of stenotic coronary artery and implications of plaque morphology on blood flow, Modeling and Simulation in Engineering, Vol. 2, No. 4, pp. 1-14.

Pankaj, M. and Surekha, J. (2013). Mathematical modeling of non-Newtonian blood flow through artery in the presence of stenosis. Advance in Applied Mathematical Biosciences, Vol 4, No. 1, pp. 1-12.

Prakash, J. and Makinde, O. D. (2011). Radiative heat transfer to blood flow through a stenotic artery in the presence of erythrocytes and magnetic field, Latin American Applied Research, Vol. 41, pp. 273-277.

Prakash, O. D., Makinde, O. D., Singh, S. P., Nidhi Jain and Deredra Kumar (2015). Effects of stenosis on non-Newtonian flow of blood in blood vessels, International Journal of Biomathematics, Vol. 8, No. 1, 1550010, 13 pages.

Puskar, R. P., Jeevan, K, Parameshwari, K. and Hari, P. G. (2020). Analysis of blood flow through artery with mild stenosis, Journal of Institute of Science and Technology, Vol. 25, No. 2, pp. 33-38.

Sapna Ratan Shah, A. and Anamika (2017). Mathematical modelling of blood flow through three-layered stenosed artery, International Jon. for Research in App. Sci. and Eng., Vol. 5, Issue VI.

Shah, S. R. and Siddiqui, S. U. (2011). Two-phase model for the study of blood flow through stenosed artery, International Journal of Pharmacy and Biological Sciences, Vol. 2, No. 1, pp. 246-254.

Sharma, B.K., Kumawat, C. and Makinde, O. D. (2022). Hemodynamical analysis of MHD two phase blood flow through a curved permeable artery having variable viscosity with heat and mass transfer, Vol. 21, pp. 797-825.

Sherwood, L. (2016). *Human physiology: From cells to systems*, Cengage Learning, USA, p. 955.

Srivastava, V. P., Mishra, S. and Rastogi, R. (2010). Non-Newtonian arterial blood flow through an overlapping stenosis, Application and Applied Mathematics, Vol. 5, No. 1, pp. 225-238.

Somchai Sriyab, (2020). The effect of stenotic geometry and non-Newtonian property of blood flow through arterial stenosis, Bentham Science, Cardiovascular and Haematological Disorder Drug Targets, Vol. 20, pp. 16-30.

Taylor. (1959). The influence of the anomalous viscosity of blood upon its oscillatory flow, Physics in Medicine and Biology, Vol. 3, No. 3, pp. 273 - 290.

Verma, V. K., Singh, M. P. and Katiyar, V. K. (2004). Analytical study of blood flow through an artery with mild stenosis, Acta Ciencia Indica, Vol. XXX M. (2), 281.

Young, D. F. (1968). Effect of a time-dependent stenosis on flow through a tube, Journal of Eng. and Ind. Trans, ASME, Vol. 9, pp. 248-254. http://doi.org/10.1115/1.3604621

Appendix

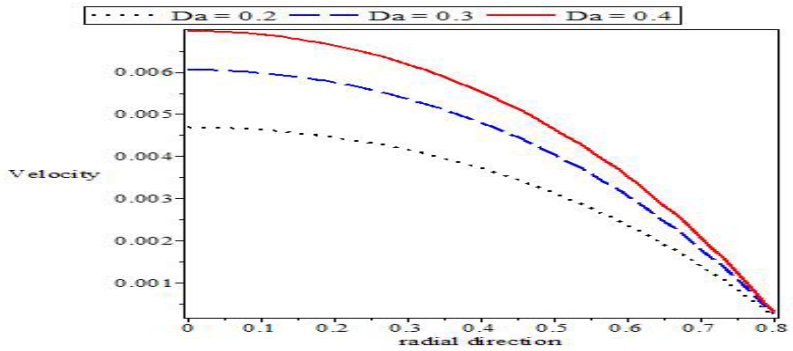

Figure 2: Velocity against r for different values of Da

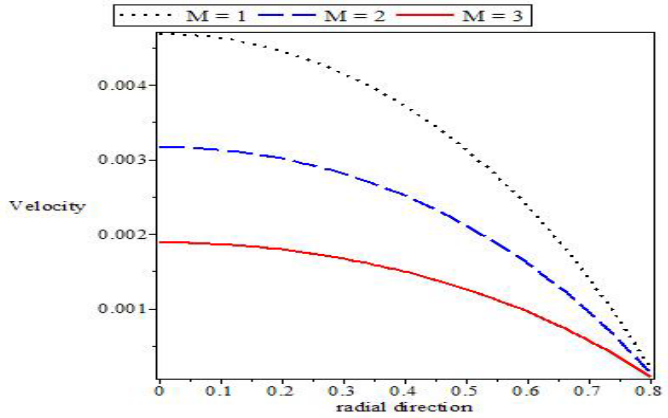

Figure 3: Velocity against r for different values of M

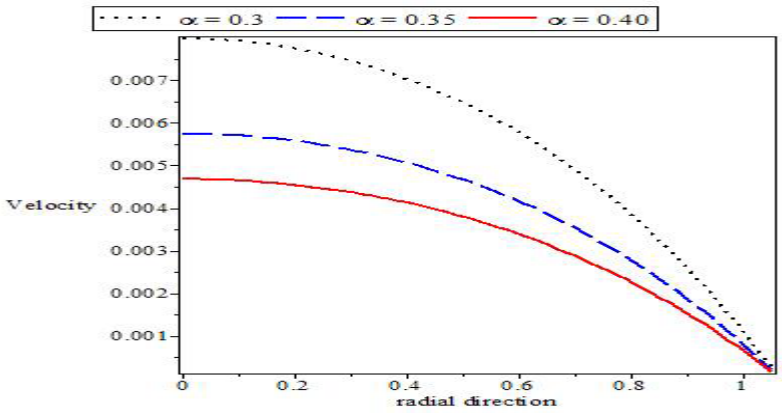

Figure 4: Velocity against r for different values α

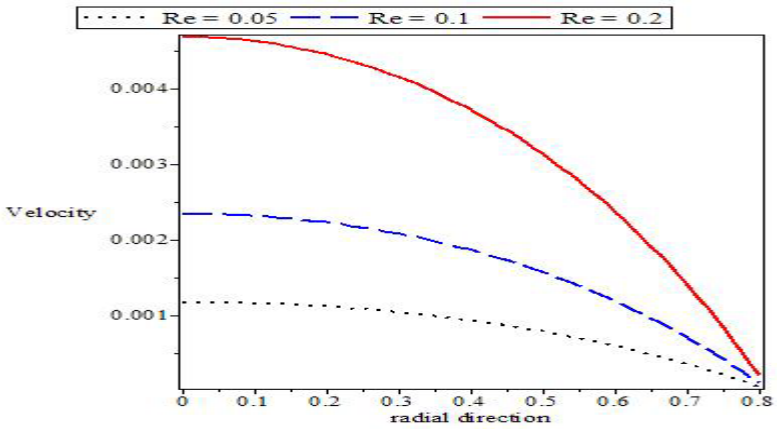

Figure 5: Velocity against r for different values of Reynold number

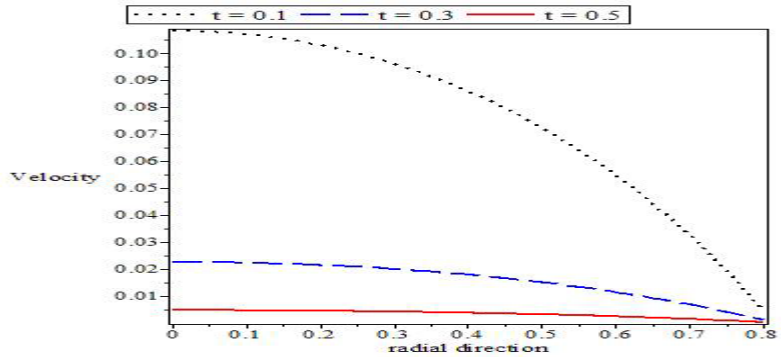

Figure 6: Velocity against r for different values of time

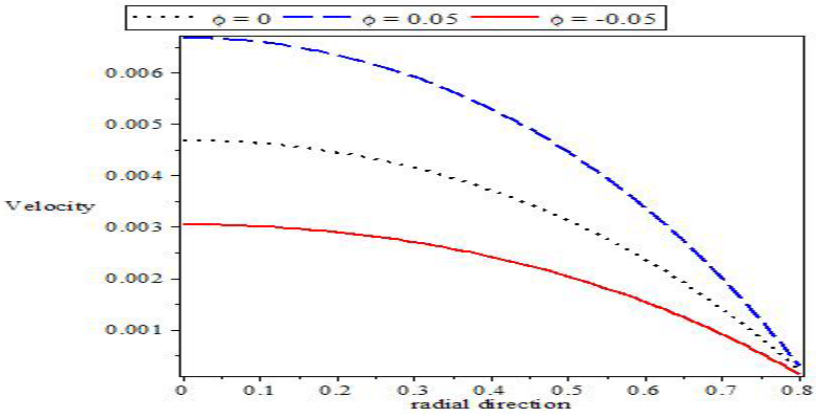

Figure 7: Velocity against r for different values of φ

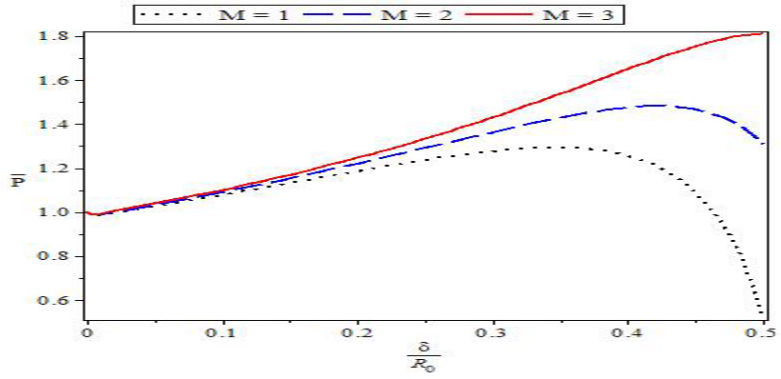

Figure 8: Pressure drop against $\frac{\delta}{R_0}$ for different values of M

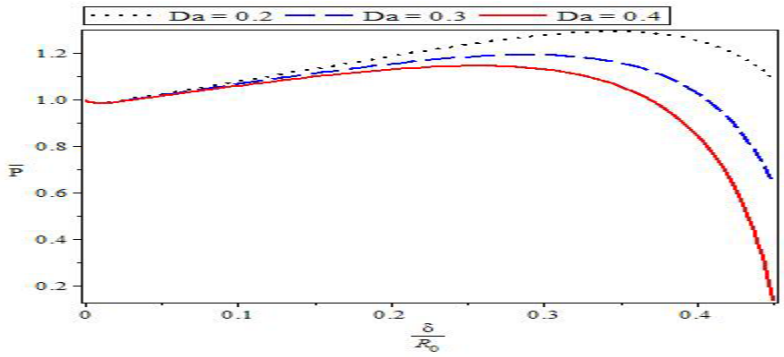

Figure 9: Pressure drop against $\frac{\delta}{R_0}$ for different values of Da

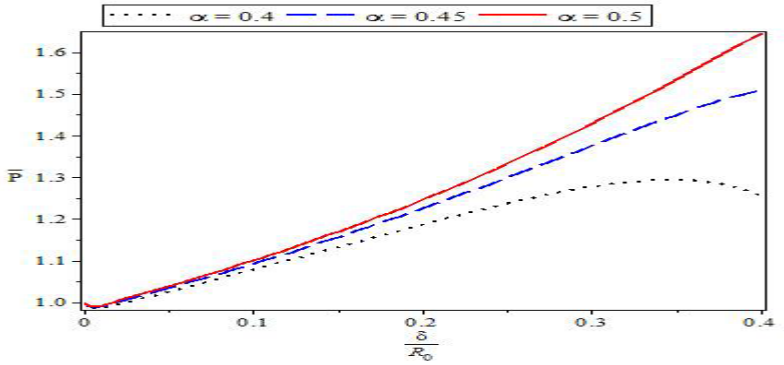

Figure 10: Pressure drop against $\frac{\delta}{R_0}$ for different values of α

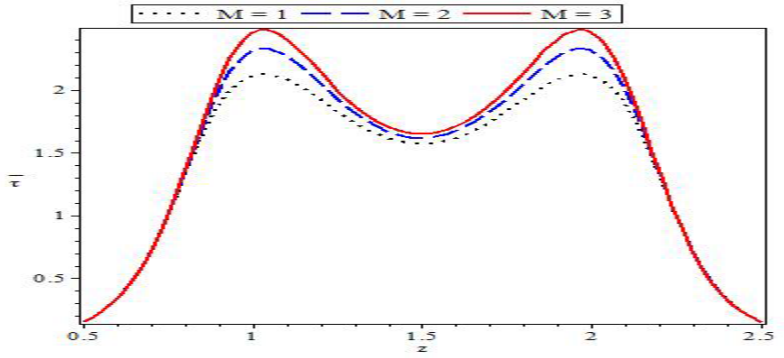

Figure 11: Wall shear stress against z for different values of M

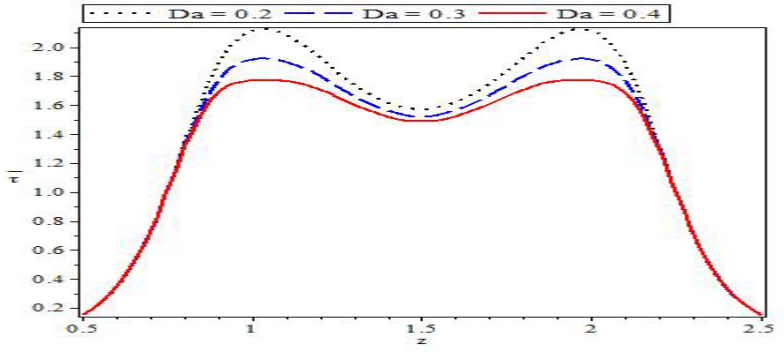

Figure 12: Wall shear stress against z for different values of Da

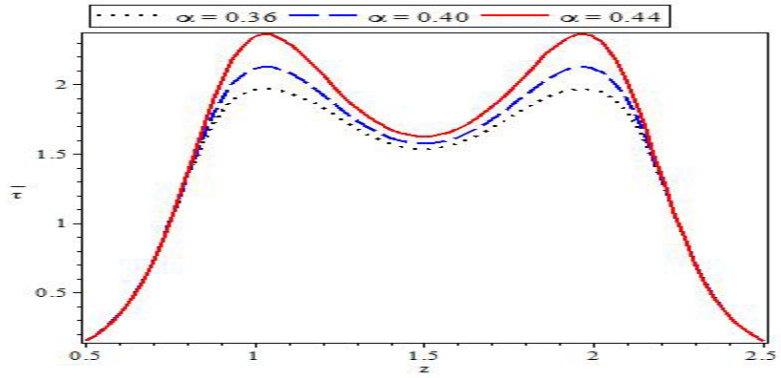

Figure 13: Wall shear stress against z for different values of α

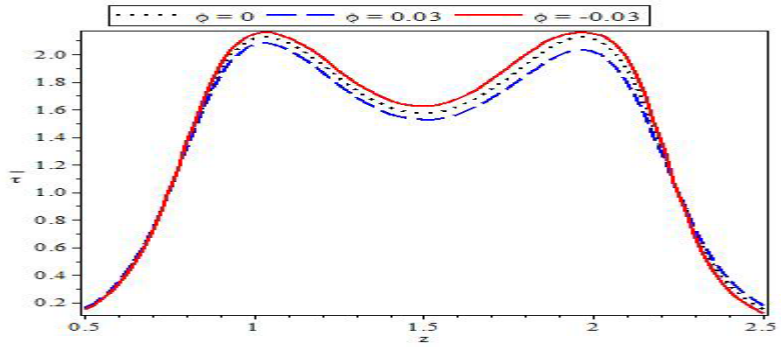

Figure 14: Wall shear stress against z for different values of φ

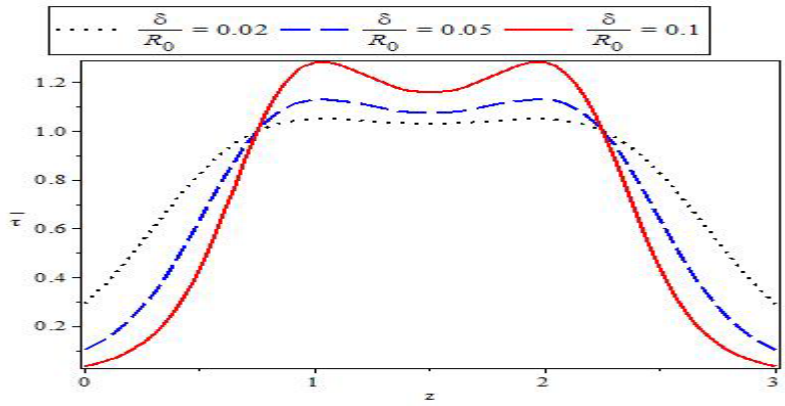

Figure 15: Wall shear stress against z for different values of $\frac{\delta}{R_0}$

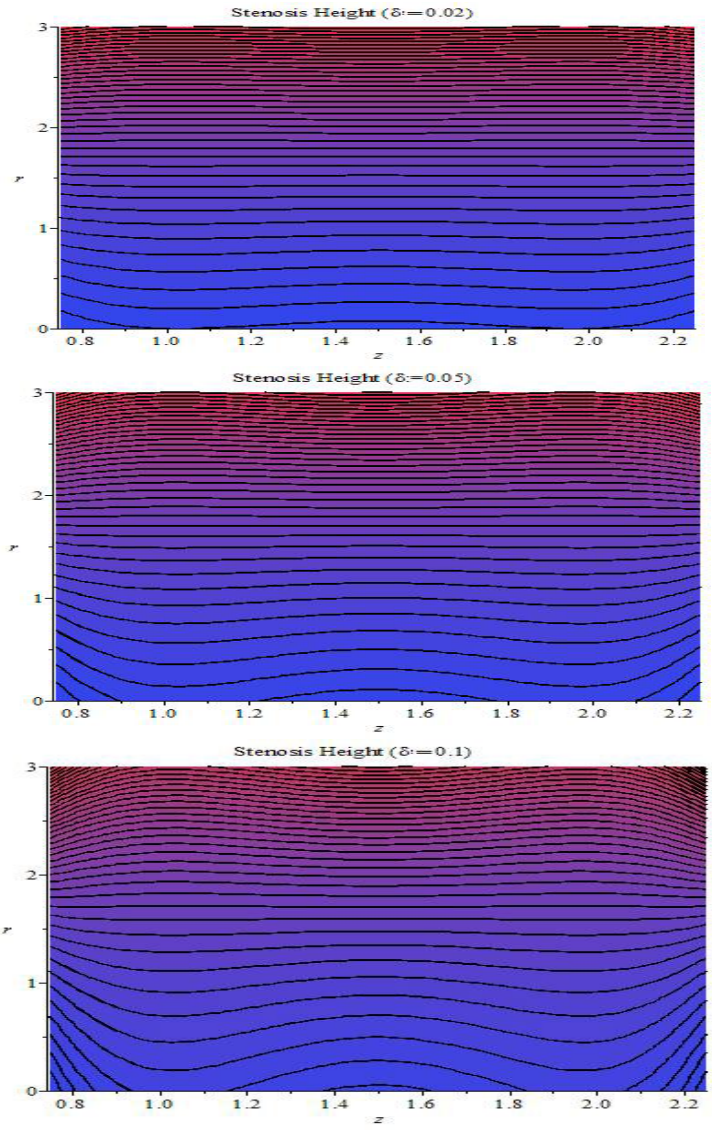

Figure 16: Streamline for $\delta = 0.02, 0.05, 0.1$

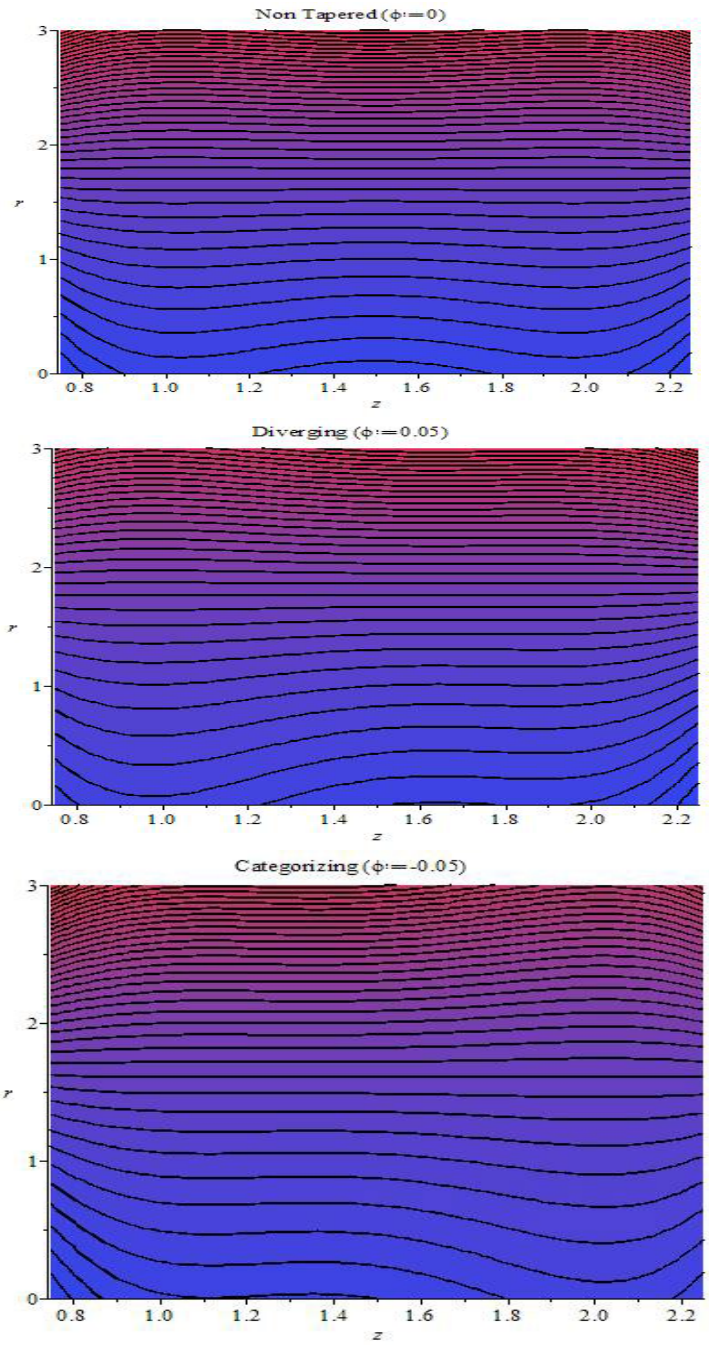

Figure 17: Streamline for $\varphi = 0, 0.05, -0.05$